THE JOURNAL OF PHYSICAL CHEMISTRY C
A JOURNAL OF THE AMERICAN CHEMICAL SOCIETY

pubs.acs.org/JPCC

Article

C_2H_2 Selective Hydrogenation to C_2H_4: Engineering the Surface Structure of Pd-Based Alloy Catalysts to Adjust the Catalytic Performance

Wenjuan Zheng,[#] Yuan Wang,[#] Baojun Wang, Maohong Fan, Lixia Ling, and Riguang Zhang*

Cite This: *J. Phys. Chem. C* 2021, 125, 15251−15261

Read Online

ACCESS | Metrics & More | Article Recommendations | Supporting Information

ABSTRACT: The surface structure of the catalyst is a key factor to affect its catalytic performance toward the targeted reaction. In this work, aiming at revealing the surface structure influences of Pd-based alloy catalysts on the catalytic performance of C_2H_2 selective hydrogenation, four kinds of surface structures of Pd-based alloy catalysts, including the core−shell Pd_{nL}@M (M = Cu and Ag), the core−shell Pd_{nL}@Pd_xM_y, the uniform alloy Pd_1Cu_3 and Pd_1Ag_1, and the subsurface structure Pd_{1L}-M_{sub} are engineered, and the corresponding catalytic performance is fully examined using DFT calculations. Our results reveal that the catalytic performance of C_2H_2 selective hydrogenation is closely related to the surface structures of Pd-based alloy catalysts; among them, the Pd_1Cu_3, Pd_{1L}-Cu_{sub}, Pd_1Ag_1, and Pd_{1L}-Ag_{sub} catalysts are screened out to serve as four promising candidates in the hydrogenation process, which exhibit better activity and selectivity toward gaseous C_2H_4 formation, especially, Pd_1Cu_3 and Pd_1Ag_1 with the uniform alloy structure. However, in the polymerization process, both Pd_{1L}-Cu_{sub} and Pd_{1L}-Ag_{sub} catalysts are deactivated due to the easier production of green oil, whereas both Pd_1Cu_3 and Pd_1Ag_1 catalysts effectively inhibit green oil production and present excellent thermal stability due to their ordered atomic arrangement. This work indicates the importance of rationally engineering the surface structure of Pd-based alloy catalysts, which may be applied to the design of other catalysts in C_2H_2 selective hydrogenation.

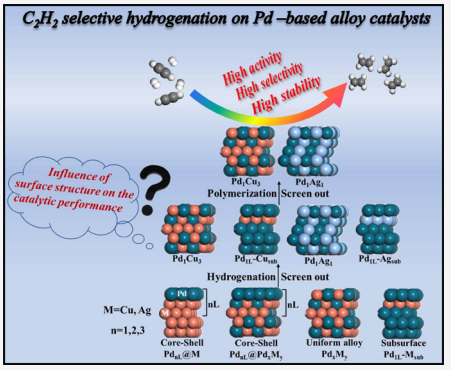

1. INTRODUCTION

In the process of C_2H_4 production by pyrolyzing petroleum hydrocarbons, trace C_2H_2 can be generated, which not only reduces the property of a C_2H_4 polymer but also leads to the catalyst deactivation in C_2H_4 polymerization due to the formation of green oil, so it is necessary to remove trace C_2H_2 from the feedstock C_2H_4.[1,2] Nowadays, C_2H_2 selective hydrogenation to C_2H_4 is an effective method to remove trace C_2H_2 from a large amount of the feedstock C_2H_4.[3,4]

Pd-based catalysts have been industrially used for C_2H_2 selective hydrogenation, such as Pd−Cu,[5−8] Pd−Ag,[9,10] Pd−Au,[11−13] Pd−Zn,[14] and Pd−In[15] catalysts; these Pd-based alloy catalysts exhibit excellent catalytic activity and C_2H_4 selectivity compared to a Pd catalyst by optimizing alloying elements. Núria and Crisa[16] summarized C_2H_2 selective hydrogenation on a large number of Pd-based catalysts modified by the second metals (Cu, Au, Ag, Zn, Ga, Sn, Pb, and Bi) and elucidated the role of the second metals. Vignola *et al.*[17] studied the adsorption of C_2H_2 on Pd−Ag alloy catalysts and found that C_2H_2 adsorption leads to the reorganization of the catalyst surface. McCue and Anderson[4] reviewed C_2H_2 selective hydrogenation on Pd-based catalysts and showed that the introduction of a second metal (Cu, Au, Ag and Ga) improves C_2H_4 selectivity by decreasing the Pd ensemble size and hindering the formation of hydrides. Ravanchi *et al.*[18] reviewed C_2H_2 selective hydrogenation on Pd-based catalysts and concluded that C_2H_4 selectivity can be improved by the addition of promoters (Ag, Na, Ga, Au, Sn, Bi, Sb, B, Ni, Cu, Pb, Cr, and K), which is attributed to the dilution of Pd active sites and the synergistic effect of the alloy. Meanwhile, the catalytic performance of Pd-based catalysts can be also adjusted by engineering the surface structure of Pd-based alloy catalysts, in which the atomic arrangement of Pd and alloying elements is changed.[19−23]

In order to rationally engineer the surface structure of Pd-based alloy catalysts, the key factor is to probe into the intrinsic surface structure characteristics of Pd-based alloy catalysts, in particular, the synergistic effect that exists between the alloying elements and the atomic arrangement, which determine the catalytic performance. For example, three kinds of PdZn alloy catalysts (the core−shell Pd@Zn, disordered PdZn, and ordered PdZn) with different atomic arrangements of both Pd and doping Zn atoms were investigated, and the influence

Received: April 8, 2021
Revised: June 23, 2021
Published: July 8, 2021

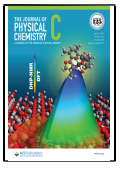

https://doi.org/10.1021/acs.jpcc.1c03157
J. Phys. Chem. C 2021, 125, 15251−15261

of different surface structures on the catalytic performance of an oxygen reduction reaction in an alkaline medium was clarified; among them, the core−shell Pd@Zn catalyst displays the best catalytic performance.[24] Kang *et al.*[25] reported HCOOH oxidation on Pt_3Pb nanocrystals; the activity can be further improved by engineering the surface structure to form the core−shell Pt_3Pb-Pt catalyst. Xie *et al.*[26] studied the influence of core−shell Pt_{nL}@Pd (n = 1−6) catalysts with different Pt shell layers on the catalytic performance in the oxygen reduction reaction; compared to a commercial Pt/C catalyst, the formed Pt_{2L}@Pd and Pt_{3L}@Pd catalysts show the highest activity. Yang *et al.*[27] theoretically investigated HCOOH dissociation on four types of surface structures of Pd-based alloy catalysts doped by the metal M (M = Cu, Au, Ag, Ir, Pt, Rh, and Ni) including the core−shell Pd@M, the core−shell Pd@Pd-M, the uniform alloy, and the subsurface structures; the results found that the core−shell Pd_{2L}@Pd_1Ag_1 and Pd_{2L}@Pd_1Au_1 exhibit the best catalytic performance toward HCOOH dissociation to hydrogen.

In C_2H_2 selective hydrogenation, Takht Ravanchi *et al.*[28] found that the core−shell Pd@Ag catalysts are more conducive to improving C_2H_4 formation activity and selectivity in comparison with the pure Pd catalyst. The experimentally prepared core−shell Pd@Au catalysts with the thicker Pd shell displays better C_2H_4 formation activity and selectivity compared to that with the thin Pd shell.[29] However, to date, to the best of our knowledge, a few studies have been systematically carried out to reveal the surface structure influences of Pd-based alloy catalysts on C_2H_4 formation activity and selectivity in C_2H_2 selective hydrogenation, in which the surface structures of Pd-based alloy catalysts are engineered by optimizing the alloying elements and altering the atomic arrangement of both Pd and alloying elements. Thus, the catalytic performance of C_2H_2 selective hydrogenation on the Pd-based alloy catalysts affected by their surface structures is still unclear.

In this study, aiming at solving above issues, C_2H_2 selective hydrogenation on Pd-based alloy catalysts with four kinds of surface structures was fully examined using density functional theory (DFT) calculations. The synergistic effect of alloying elements and the different atomic arrangements with the surface layer Pd and alloying elements to form different surface structures are considered. Two commonly used alloying elements Cu and Ag and the corresponding four types of atomic arrangements are investigated for Pd-based alloy catalysts. The obtained results are expected to illustrate the importance of rationally engineering the surface structure of Pd-based catalysts in adjusting their catalytic performance toward C_2H_2 selective hydrogenation, which may be applied to the design of other types of catalysts.

2. COMPUTATIONAL DETAILS

2.1. Computational Methods. All DFT calculations in this study were implemented using the Dmol^3 code[30,31] in Materials Studio 8.0. The generalized gradient approximation (GGA) and Perdew−Burke−Ernzerhof (PBE) functionals[32,33] were applied to treat the exchange−correlation potential. The effective core potential (ECP) basis set was performed for Pd-based alloy catalysts, and the all-electron basis set was applied to other nonmetallic species. The valence wave functions were expanded by the double-numeric polarized (DNP) basis set.[34,35] The k-points of 3 × 3 × 1 were used to handle surface models. A smearing width is 0.005 Ha. The transition states of C_2H_2 selective hydrogenation were obtained by the complete linear synchronous transit/quadratic synchronous transit (LST/QST) technique.[36,37] TS confirmation and frequency analysis were further carried out to verify the accuracy of the transition state.

C_2H_2 selective hydrogenation on the Pd-based catalysts usually occurs at the temperature of 300−500 K under the experimental conditions;[38,39] thus, all energies involved in the adsorption and the reaction were calculated at 425 K to consider the entropy and thermal contribution.

2.2. Surface Models. In this study, for the uniform alloy Pd_xM_y (M = Cu and Ag), Wang *et al.*[40] showed that the uniform alloy Pd_xCu_y with the Pd/Cu ratio of 1/3 has superior catalytic performance than other Pd/Cu ratios toward C_2H_2 selective hydrogenation to C_2H_4. Wang *et al.*[41] also found that the uniform alloy Pd_xAg_y with the Pd/Ag ratio of 1/1 has superior catalytic performance compared to other Pd/Ag ratios in C_2H_2 selective hydrogenation. Thus, the Pd/Cu ratio of 1/3 and the Pd/Ag ratio of 1/1 for the uniform alloy Pd_xM_y (M = Cu, Ag) are considered, and the corresponding optimized lattice parameters are 3.73 and 4.04 Å, respectivey, which are close to the previously reported values of 3.70 and 3.98 Å,[42] respectively. Based on the low surface energy and the mainly exposed surface,[43−48] the (111) surfaces with a five-layer $p(3 \times 3)$ supercell are constructed to model the pure metals Pd, Cu, and Ag and the uniform alloy Pd_1Cu_3 and Pd_1Ag_1 catalysts.

Aiming at revealing the influence of the atomic arrangement of Pd-based alloy catalysts, four types of atomic arrangements were constructed in this study; the first is the core−shell Pd_{nL}@M (M = Cu and Ag) catalysts obtained by replacing one, two, and three layers of Cu or Ag catalysts with Pd atoms, named as Pd_{1L}@M, Pd_{2L}@M, and Pd_{3L}@M (M = Cu and Ag), respectively; the second is the core−shell Pd_{nL}@Pd_xM_y (M = Cu and Ag) catalysts obtained by replacing one, two, and three layers of the Pd_1Cu_3 or Pd_1Ag_1 catalyst with Pd atoms, named as Pd_{1L}@Pd_xM_y, Pd_{2L}@Pd_xM_y, and Pd_{3L}@Pd_xM_y (M = Cu and Ag), respectively; the third is the uniform alloy Pd_1Cu_3 and Pd_1Ag_1 catalysts; the fourth is the subsurface structure Pd_{1L}-M_{sub} (M = Cu and Ag) catalysts obtained by replacing the subsurface layer of the Pd catalyst with Cu or Ag atoms, named as Pd_{1L}-Cu_{sub} or Pd_{1L}-Ag_{sub}, respectively.

Above constructed catalyst models were optimized; during the optimization, the bottom two layers of all catalysts are fixed, and the top three layers are relaxed. A vacuum of 15 Å is set to separate the periodic slabs. All the optimized catalyst models are shown in Figure 1.

2.3. The Calculations of Gibbs Free Energy. The adsorption free energy (G_{ads}) is calculated according to eq 1:

$$G_{ads} = E_{system} + G_{system} - (E_{catal} + G_{catal} + E_{adsorbate} + G_{adsorbate}) \quad (1)$$

where E_{system} is the total energy adsorbed of the system in its equilibrium state, E_{catal} is the total energy of the clean catalyst, and $E_{adsorbate}$ is the total energy of the gas-phase adsorbate; G_{catal}, $G_{adsorbate}$, and G_{system} are the corresponding corrections of free energies at 425 K. According to this definition, the more negative the value of G_{ads} is, the stronger the adsorption ability of the adsorbed species on the surface is.

The activation free energy (G_a) and reaction free energy (ΔG) are calculated on the basis of eqs 2 and 3.

$$G_a = E_{TS} + G_{TS} - E_{IS} - G_{IS} \quad (2)$$

https://doi.org/10.1021/acs.jpcc.1c03157
J. Phys. Chem. C 2021, 125, 15251−15261

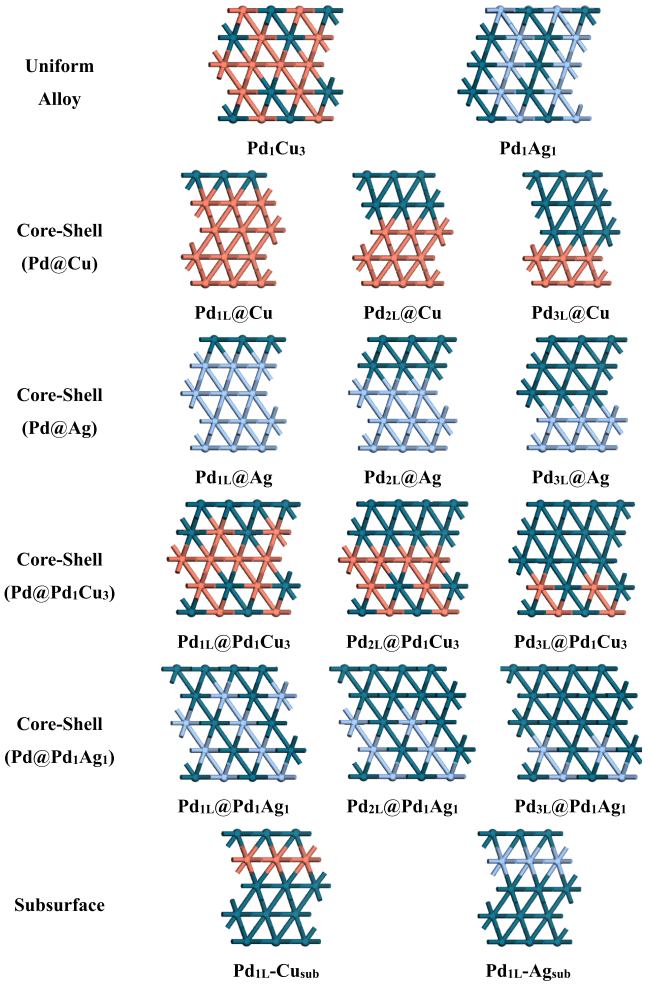

Figure 1. Constructed catalyst models considered in this study.

$$\Delta G = E_{FS} + G_{FS} - E_{IS} - G_{IS} \quad (3)$$

where E_{IS}, E_{TS}, and E_{FS} represent the total energies of the initial state (IS), the transition state (TS), and the final state (FS), respectively; G_{IS}, G_{TS}, and G_{FS} correspond to the corrections of the free energies at 425 K. In our calculation, the values of G_{IS}, G_{TS}, and G_{FS} at a finite temperature (425 K) can be directly obtained from the data in the DMol[3] output document of frequency analysis.

3. RESULTS AND DISCUSSION

3.1. The Possible Reaction Routes of C_2H_2 Selective Hydrogenation. As presented in Figure 2, C_2H_2 selective hydrogenation includes two processes of the hydrogenation and polymerization.

In the hydrogenation process, three possible routes exist; the first is a ***C_2H_4desorption route*** in which C_2H_2(ad) is first hydrogenated via a C_2H_3(ad) intermediate to generate C_2H_4(ad), followed by its desorption from the catalyst surface; the second is a ***C_2H_4hydrogenation route*** in which C_2H_2(ad) is excessively hydrogenated to C_2H_5(ad) via a C_2H_4 intermediate; the third is a ***$CHCH_3$hydrogenation route*** in which C_2H_2(ad) is excessively hydrogenated to C_2H_5(ad) via a $CHCH_3$ intermediate. The route of C_2H_4 desorption is expected to be dominant to realize the removal of trace C_2H_2 in C_2H_4-rich stream. Thus, it is needed to first determine the preference between C_2H_4 hydrogenation and its desorption; then, when the C_2H_4 desorption route is favored, starting from the common intermediate C_2H_3 in three routes, the superiority between the C_2H_4 desorption route and the $CHCH_3$ hydrogenation route is further judged; finally, the catalysts that can produce gaseous C_2H_4 in three routes are screened out.

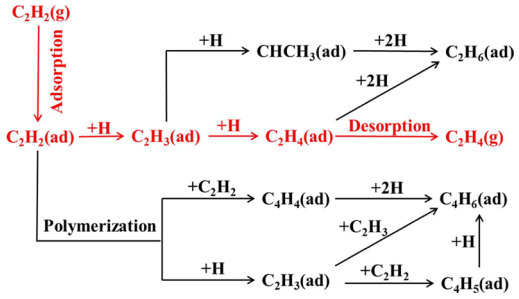

Figure 2. Possible reaction pathways of C_2H_2 selective hydrogenation including the hydrogenation and polymerization processes: (ad) stands for the adsorbed state and (g) stands for the gas-phase state.

In the polymerization process, green oil is produced to block active centers and deactivate the catalysts. Most studies have shown that 1,3-butadiene is the precursor for the production of green oil (the liquid part of C_{4+} hydrocarbons);[2,49] when the formation of 1,3-butadiene is inhibited, the formation of green oil can be inhibited. Thus, green oil refers to 1,3-butadiene in this study. As a result, three possible routes of 1,3-butadiene production are investigated; the first is the coupling of adsorbed C_2H_2 to C_4H_4, followed by its hydrogenation to C_4H_6; the second is the coupling of adsorbed C_2H_2 and C_2H_3 to C_4H_5, followed by its hydrogenation to C_4H_6; the third is the coupling of adsorbed C_2H_3 to C_4H_6.

3.2. The Adsorption of H and C_2H_x (x = 2−5) Species. For the core−shell Pd_{2L}@Cu and Pd_{3L}@Cu catalysts, as presented in Figure S2, our results show that when H and C_2H_x (x = 2−5) species are adsorbed, the surfaces of Pd_{2L}@Cu and Pd_{3L}@Cu are severely deformed after geometry optimization; further, the surfaces of Pd_{2L}@Cu and Pd_{3L}@Cu catalysts with the co-adsorption of H and C_2H_x (x = 2−5) species still undergo severe deformation (see Figure S3), so the surfaces of Pd_{2L}@Cu and Pd_{3L}@Cu catalysts are unstable in C_2H_2 selective hydrogenation, which are not considered in this study. For the surfaces of other 14 types of Pd-based alloy catalysts, the most stable adsorption configurations of H and C_2H_x (x = 2−5) are presented in Figure S4 and the adsorption free energies are listed in Table S1.

Since the amount of C_2H_2 in the C_2H_4-rich stream is small, C_2H_2 must be strongly adsorbed on the catalyst than C_2H_4 to ensure C_2H_2 hydrogenation. Thus, the difference between the adsorption abilities of C_2H_2 and C_2H_4 species is analyzed. As presented in Figure 3, for 10 types of core−shell Pd-based alloy catalysts, C_2H_2 adsorption is much stronger than C_2H_4 adsorption (kJ·mol^{-1}) on Pd_{1L}@Cu (−114.4 *vs* −49.8), Pd_{1L}@Pd_1Cu_3 (−112.8 *vs* −40.9), Pd_{2L}@Pd_1Cu_3 (−149.5 *vs* −73.5), Pd_{3L}@Pd_1Cu_3 (−145.5 *vs* −69.8), Pd_{1L}@Ag (−152.2 *vs* −55.7), Pd_{2L}@Ag (−189.0 *vs* −77.4), Pd_{3L}@Ag (−183.4 *vs* −71.9), Pd_{1L}@Pd_1Ag_1 (−175.2 *vs* −71.5), Pd_{2L}@Pd_1Ag_1 (−181.1 *vs* −71.8), and Pd_{3L}@Pd_1Ag_1 (−176.9 *vs* −71.3). For the uniform alloy and subsurface structure catalysts, C_2H_2 has a much larger adsorption energy (kJ·mol^{-1}) than C_2H_4 on Pd_1Cu_3 (−116.1 *vs* −45.5), Pd_1Ag_1 (−117.5 *vs* −49.3), Pd_{1L}-Cu_{sub} (−121.0 *vs* −40.2), and Pd_{1L}-Ag_{sub} (−140.3 *vs* −58.4).

https://doi.org/10.1021/acs.jpcc.1c03157
J. Phys. Chem. C 2021, 125, 15251−15261

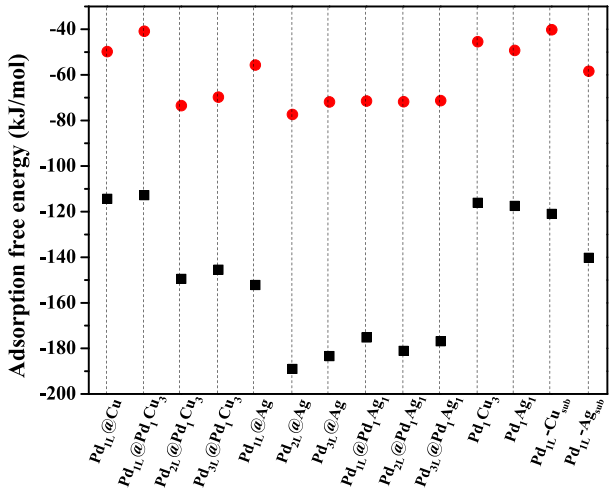

Figure 3. Adsorption free energies of C_2H_2 (black square) and C_2H_4 (red circle) species on the Pd-based alloy catalysts at 425 K.

Thus, the hydrogenation of C_2H_2 can be performed on these 14 types of Pd-based alloy catalysts.

3.3. Influences of Surface Structures on H_2 Dissociation. Since H_2 dissociation is the key initial step for C_2H_2 selective hydrogenation, H_2 adsorption and dissociation were further investigated over above 14 types of Pd-based alloy catalysts (see Figures S5 and S6), suggesting that H_2 dissociative adsorption proceeds spontaneously on the core−shell Pd_{1L}@Cu, Pd_{1L}@Pd_1Cu_3, Pd_{2L}@Pd_1Cu_3, Pd_{3L}@Pd_1Cu_3, Pd_{1L}@Ag, Pd_{2L}@Ag, Pd_{3L}@Ag, Pd_{1L}@Pd_1Ag_1, Pd_{2L}@Pd_1Ag_1, and Pd_{3L}@Pd_1Ag_1, as well as the subsurface structure of Pd_{1L}-Cu_{sub} and Pd_{1L}-Ag_{sub} catalysts. However, H_2 molecular adsorption occurs on the uniform alloy Pd_1Cu_3 and Pd_1Ag_1, while the activation barriers of H_2 dissociation are 19.7 and 19.6 kJ·mol^{-1}, respectively, namely, both Pd_1Cu_3 and Pd_1Ag_1 catalysts also promote H_2 dissociation to form adsorbed H atoms.

Based on above results, among above 14 types of Pd-based alloy catalysts, the dissociation of H_2 into an H atom can easily occur, which can provide an abundant hydrogen source to participate into the C_2H_2 hydrogenation reaction.

3.4. Influences of Surface Structures on the Preference between C_2H_4 Desorption and Its Hydrogenation. The preference between C_2H_4 hydrogenation and its desorption is further examined on above 14 types of Pd-based catalysts, as shown in Figures 4−6.

For the core−shell Pd-based alloy catalysts, C_2H_4 prefers to desorb rather than its hydrogenation to C_2H_5 on Pd_{1L}@Cu (49.8 *vs* 93.9 kJ·mol^{-1}, Figure 4a), Pd_{1L}@Pd_1Cu_3 (40.9 *vs* 95.6 kJ·mol^{-1}, Figure 4b), Pd_{2L}@Pd_1Cu_3 (73.5 *vs* 92.7 kJ·mol^{-1}, Figure 4c), Pd_{3L}@Pd_1Cu_3 (69.8 *vs* 87.1 kJ·mol^{-1}, Figure 4d), Pd_{1L}@Ag (55.7 *vs* 111.8 kJ·mol^{-1}, Figure 5a), Pd_{2L}@Ag (77.4 *vs* 106.7 kJ·mol^{-1}, Figure 5b), Pd_{3L}@Ag (71.9 *vs* 106.9 kJ·mol^{-1}, Figure 5c), Pd_{1L}@Pd_1Ag_1 (71.5 *vs* 114.4 kJ·mol^{-1}, Figure 5d), Pd_{2L}@Pd_1Ag_1 (71.8 *vs* 99.6 kJ·mol^{-1}, Figure 5e), and Pd_{3L}@Pd_1Ag_1 (71.3 *vs* 103.4 kJ·mol^{-1}, Figure 5f). The same things also occur on the uniform alloy and subsurface structure catalysts, including Pd_1Cu_3 (45.5 *vs* 97.4, Figure 6a), Pd_1Ag_1 (49.3 *vs* 108.9, Figure 6b), Pd_{1L}-Cu_{sub} (40.2 *vs* 95.1, Figure 6c), and Pd_{1L}-Ag_{sub} (58.4 *vs* 88.0, Figure 6d). Thus, C_2H_4 desorption prefers to occur in kinetics instead of its hydrogenation over these 14 types of Pd-based alloy catalysts.

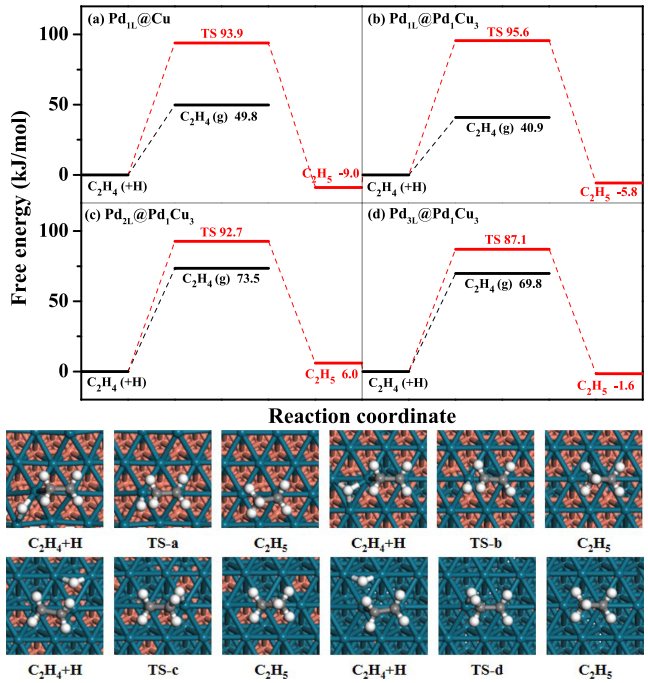

Figure 4. Free-energy profile of C_2H_4 hydrogenation and C_2H_4 desorption with the initial state, transition state, and the final state on Pd_{1L}@Cu and Pd_{nL}@Pd_1Cu_3(n = 1−3) at 425 K.

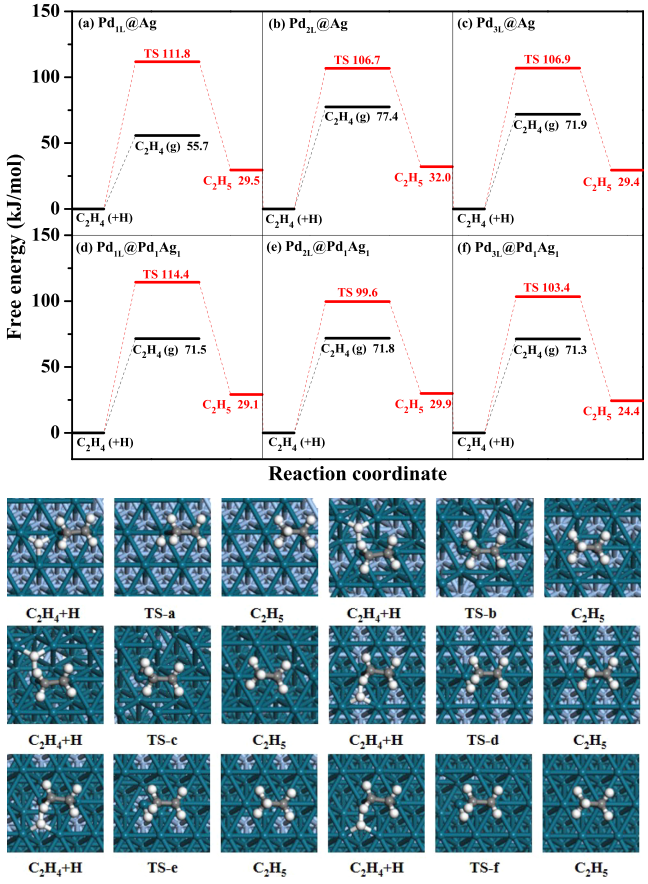

Figure 5. Free-energy profile of C_2H_4 hydrogenation and C_2H_4 desorption with the initial state, transition state, and the final state on Pd_{nL}@Ag and Pd_{nL}@Pd_1Ag_1(n = 1−3) at 425 K.

https://doi.org/10.1021/acs.jpcc.1c03157
J. Phys. Chem. C 2021, 125, 15251−15261

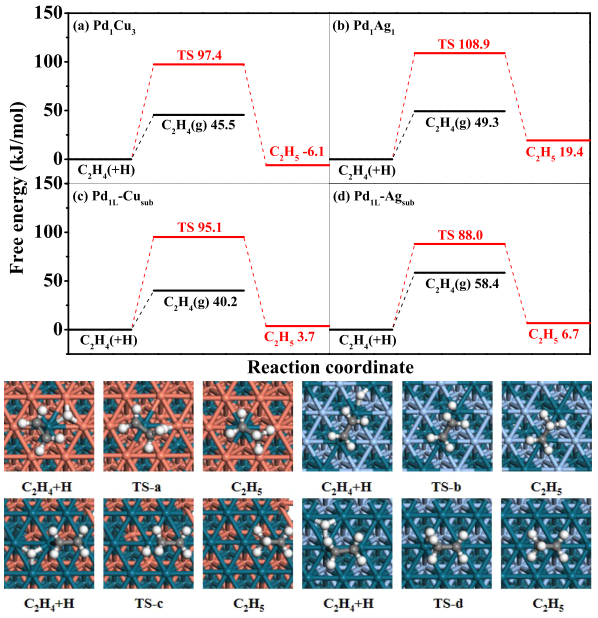

Figure 6. Free-energy profile of C_2H_4 hydrogenation and C_2H_4 desorption with the initial state, transition state, and the final state on Pd_1Cu_3, Pd_1Ag_1, Pd_{1L}-Cu_{sub}, and Pd_{1L}-Ag_{sub} catalysts at 425 K.

3.5. Influences of Surface Structures on the Preference between C_2H_4 Desorption and $CHCH_3$ Hydrogenation Routes.

Starting from the common intermediate C_2H_3, we further determine whether the C_2H_4 desorption route is also easier in kinetics than the $CHCH_3$ hydrogenation route.

As shown in Figure 7, take Pd_{1L}@Cu as an example, the $CHCH_3$ hydrogenation route is kinetically favored compared to the C_2H_4 desorption route (86.2 *vs* 94.7 kJ·mol^{-1}); thus, Pd_{1L}@Cu is beneficial to C_2H_5 formation, followed by its hydrogenation to ethane.

For the Pd_{nL}@Pd_1Cu_3 (n = 1−3) catalysts, C_2H_3 is preferentially hydrogenated to C_2H_4 instead of $CHCH_3$ on Pd_{1L}@Pd_1Cu_3 (84.6 *vs* 111.9 kJ·mol^{-1}, Figure S7a), so the $CHCH_3$ hydrogenation route does not occur. On Pd_{2L}@Pd_1Cu_3, the C_2H_4 desorption route is kinetically favored compared to the $CHCH_3$ hydrogenation route (99.7 *vs* 159.2 kJ·mol^{-1}, Figure S7b). However, on Pd_{3L}@Pd_1Cu_3, the $CHCH_3$ hydrogenation route is kinetically favored compared to the C_2H_4 desorption route (100.4 *vs* 146.8 kJ·mol^{-1}, Figure S7c). Thus, both Pd_{1L}@Pd_1Cu_3 and Pd_{2L}@Pd_1Cu_3 are beneficial to the C_2H_4 desorption route to form gaseous C_2H_4, while Pd_{3L}@Pd_1Cu_3 is beneficial to C_2H_5 formation, followed by its hydrogenation to ethane.

For the Pd_{nL}@Ag (n = 1−3) catalysts, C_2H_3 hydrogenation to C_2H_4 is more favored in kinetics compared to its hydrogenation to $CHCH_3$ on Pd_{1L}@Ag (116.0 *vs* 178.9 kJ·mol^{-1}, Figure S8a), so the C_2H_4 desorption route is dominant. The C_2H_4 desorption route is kinetically favored than the $CHCH_3$ hydrogenation route on Pd_{2L}@Ag (148.5 *vs* 196.8 kJ·mol^{-1}, Figure S8b) and Pd_{3L}@Ag (126.0 *vs* 188.4 kJ·mol^{-1}, Figure S8c). Thus, Pd_{nL}@Ag (n = 1−3) favor the C_2H_4 desorption route to form gaseous C_2H_4.

For the Pd_{nL}@Pd_1Ag_1 (n = 1−3) catalysts, the C_2H_4 desorption route is kinetically favored compared to the $CHCH_3$ hydrogenation route on Pd_{1L}@Pd_1Ag_1 (139.9 *vs* 182.5 kJ·mol^{-1}, Figure S9a) and Pd_{3L}@Pd_1Ag_1 (111.9 *vs* 193.3 kJ·mol^{-1}, Figure S9c), respectively. However, on Pd_{2L}@Pd_1Ag_1, the $CHCH_3$ hydrogenation route is kinetically favored compared to the C_2H_4 desorption route (177.4 *vs* 195.5 kJ·mol^{-1}, Figure S9b). Thus, both Pd_{1L}@Pd_1Ag_1 and Pd_{3L}@Pd_1Ag_1 are beneficial to C_2H_4 desorption, while Pd_{2L}@Pd_1Ag_1 results in C_2H_5 formation, followed by its hydrogenation to ethane.

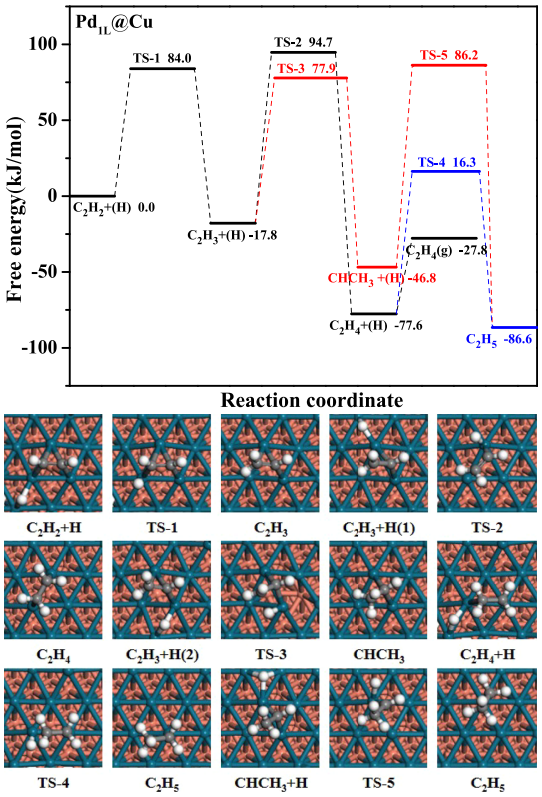

Figure 7. Free-energy profile of C_2H_2 selective hydrogenation with the initial states, transition states, and final states on the Pd_{1L}@Cu catalyst at 425 K.

For the Pd_1Cu_3 and Pd_1Ag_1 catalysts, C_2H_3 hydrogenation to C_2H_4 is kinetically more favorable than its hydrogenation to $CHCH_3$ on Pd_1Cu_3 (14.4 *vs* 175.5, Figure S10a) and Pd_1Ag_1 (65.9 *vs* 121.5, Figure S10b); thus, both Pd_1Cu_3 and Pd_1Ag_1 dominantly contribute to the C_2H_4 desorption route to form gaseous C_2H_4.

For the Pd_{1L}-M_{sub} (M = Cu and Ag) catalysts, $C_2H_3 + H \rightarrow C_2H_4$ and $C_2H_3 + H \rightarrow CHCH_3$ are energetically competitive on the Pd_{1L}-Cu_{sub} catalyst (81.6 *vs* 84.7 kJ·mol^{-1}, Figure S11a), while C_2H_4 desorption is more kinetically favored compared to $CHCH_3$ hydrogenation (40.2 *vs* 120.6 kJ·mol^{-1}, Figure S11a). On the Pd_{1L}-Ag_{sub} catalyst, C_2H_3 hydrogenation to C_2H_4 is kinetically more favorable than its hydrogenation to $CHCH_3$ (93.4 *vs* 127.7, Figure S11b). Thus, Pd_{1L}-M_{sub} (M = Cu and Ag) catalysts are beneficial to C_2H_4 desorption.

Therefore, the $CHCH_3$ hydrogenation route is the preferred route on Pd_{1L}@Cu, Pd_{3L}@Pd_1Cu_3, and Pd_{2L}@Pd_1Ag_1, which dominantly produce ethane. However, the C_2H_4 desorption route is preferred on other 11 types of Pd-based catalysts (Pd_{1L}@Pd_1Cu_3, Pd_{2L}@Pd_1Cu_3, Pd_{1L}@Ag, Pd_{2L}@Ag, Pd_{3L}@Ag, Pd_{1L}@Pd_1Ag_1, Pd_{3L}@Pd_1Ag_1, Pd_1Cu_3, Pd_1Ag_1, Pd_{1L}-Cu_{sub}, and Pd_{1L}-Ag_{sub}), which mainly contribute to gaseous C_2H_4 formation. Namely, these 11 types of Pd-based alloy catalysts can effectively remove trace C_2H_2 from the C_2H_4-rich stream.

https://doi.org/10.1021/acs.jpcc.1c03157
J. Phys. Chem. C 2021, 125, 15251−15261

3.6. General Discussions. *3.6.1. Influences of Surface Structures on C_2H_4 Formation Activity and Selectivity.* Since 11 types of Pd-based catalysts favor gaseous C_2H_4 formation, C_2H_4 formation activity and selectivity over these catalysts are calculated to evaluate the catalytic performance of C_2H_2 selective hydrogenation.[42,50,51]

In this study, when the route of C_2H_4 desorption is favored, the energy difference between C_2H_4 desorption and its hydrogenation as the simplest descriptor is employed to quantitatively evaluate C_2H_4 selectivity.[52−54] Meanwhile, the rate of C_2H_4 formation is calculated to evaluate the activity of C_2H_4 formation,[55,56] which is calculated according to the two-step model[57,58] under the typical experimental conditions (T = 425 K, P = 1 atm; H_2/C_2H_2 = 10/1, the partial pressures of C_2H_4, H_2, and C_2H_2 correspond to 0.89, 0.1, and 0.01 atm, respectively). The details about the definition of activity and selectivity of C_2H_4 formation are presented in the Supporting Information. Further, as mentioned above, different alloying elements and atomic arrangement lead to different surface structures of Pd-based alloy catalysts and therefore alter the selectivity and activity of gaseous C_2H_4 formation.

As presented in Figure 8a, for the Pd−Cu alloy catalysts, C_2H_4 selectivity is 54.7 and 19.2 kJ·mol^{-1} on the core−shell

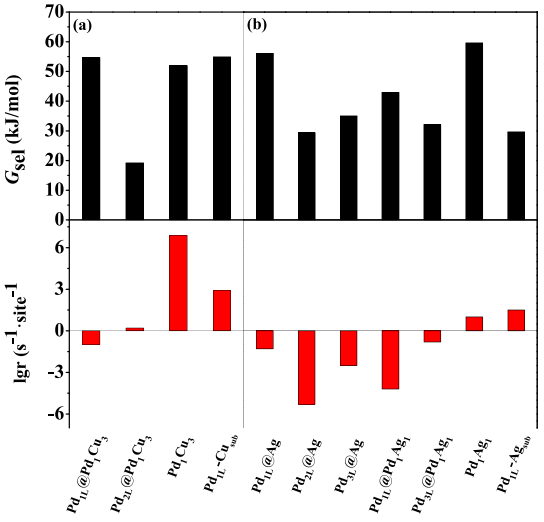

Figure 8. C_2H_4 selectivity and its formation activity in C_2H_2 selective hydrogenation on the (a) Pd−Cu and (b) Pd−Ag alloy catalysts at 425 K.

$Pd_{1L}@Pd_1Cu_3$ and $Pd_{2L}@Pd_1Cu_3$, respectively; the activity is 1.08×10^{-1} and 1.46×10^{0} s^{-1}·site^{-1}; C_2H_4 selectivity of the former is about two times higher than that of the latter; however, the activity of the latter is about nine times higher than that of the former; Thus, taking C_2H_4 formation activity and selectivity into consideration, $Pd_{2L}@Pd_1Cu_3$ is a more suitable choice for C_2H_2 selective hydrogenation to produce gaseous C_2H_4. For the uniform alloy Pd_1Cu_3, the activity and selectivity of gaseous C_2H_4 formation are 8.65×10^{6} s^{-1}·site^{-1} and 51.9 kJ·mol^{-1}, respectively. For the subsurface structure of the Pd_{1L}-Cu_{sub} catalyst, the activity and selectivity of gaseous C_2H_4 formation are 8.28×10^{2} s^{-1}·site^{-1} and 54.9 kJ·mol^{-1}, respectively. Therefore, three types of Pd−Cu alloy catalysts, including $Pd_{2L}@Pd_1Cu_3$, Pd_1Cu_3, and Pd_{1L}-Cu_{sub} with different surface structures, are more conducive to gaseous C_2H_4 formation, especially Pd_1Cu_3 (the highest activity) and Pd_{1L}-Cu_{sub} (the highest selectivity) catalysts.

Further, aiming at clarifying the role of different surface structures for Pd-Cu alloy catalysts, we calculated the projected density of states for the *d*-orbitals of the outermost atoms and the average Bader charge of the outermost Pd atoms over $Pd_{2L}@Pd_1Cu_3$, Pd_1Cu_3, and Pd_{1L}-Cu_{sub} with better catalytic performance, in which $Pd_{2L}@Pd_1Cu_3$ has a lower catalytic performance compared to the Pd_1Cu_3 and Pd_{1L}-Cu_{sub} catalysts. Further, although C_2H_4 selectivity on Pd_1Cu_3 is close to that on Pd_{1L}-Cu_{sub}, the activity of Pd_1Cu_3 is higher by about 10^4 times than that of Pd_{1L}-Cu_{sub}, thus taking C_2H_4 formation activity and selectivity into consideration; Pd_1Cu_3 shows the best catalytic performance. As presented in Figure 9a, the distance between the Femi level and the *d*-band center follows the order Pd_{1L}-Cu_{sub} (−1.96 eV) < Pd_1Cu_3 (−2.12 eV) < $Pd_{2L}@Pd_1Cu_3$ (−2.18 eV), indicating that Pd_1Cu_3 with a moderate *d*-band center exhibits superior activity than $Pd_{2L}@Pd_1Cu_3$ and Pd_{1L}-Cu_{sub}. Moreover, Bader charges of the outermost Pd atoms are −0.343 *e*, −0.126 *e*, and −0.031 *e* on Pd_1Cu_3, Pd_{1L}-Cu_{sub}, and $Pd_{2L}@Pd_1Cu_3$, respectively; namely, Pd_1Cu_3 with more Bader charges of the outermost Pd atoms presents the best catalytic performance toward gaseous C_2H_4 formation.

As shown in Figure 8b, for Pd−Ag alloy catalysts, on the $Pd_{nL}@Ag$ and $Pd_{nL}@Pd_1Ag_1$ (n = 1−3) catalysts, C_2H_4 selectivity (kJ·mol^{-1}) is ordered as $Pd_{1L}@Ag$ (56.1) > $Pd_{1L}@Pd_1Ag_1$ (42.9) > $Pd_{3L}@Ag$ (35.0) > $Pd_{3L}@Pd_1Ag_1$ (32.1) > $Pd_{2L}@Ag$ (29.3), while the activity (s^{-1}·site^{-1}) of gaseous C_2H_4 formation is in the sequence of $Pd_{3L}@Pd_1Ag_1$ (1.56×10^{-1}) > $Pd_{1L}@Ag$ (4.89×10^{-2}) > $Pd_{3L}@Ag$ (2.89×10^{-3}) > $Pd_{1L}@Pd_1Ag_1$ (5.65×10^{-5}) > $Pd_{2L}@Ag$ (4.96×10^{-6}); thus, taking C_2H_4 formation activity and selectivity into consideration, $Pd_{3L}@Pd_1Ag_1$ enables superior catalytic performance for gaseous C_2H_4 formation. For the uniform alloy Pd_1Ag_1, the activity and selectivity of gaseous C_2H_4 formation are 1.09×10^{1} s^{-1}·site^{-1} and 59.6 kJ·mol^{-1}, respectively. For the subsurface structure of Pd_{1L}-Ag_{sub}, the activity and selectivity of gaseous C_2H_4 formation are 2.93×10^{1} s^{-1}·site^{-1} and 29.6 kJ·mol^{-1}, respectively. Above results show that three types of Pd−Ag alloy catalysts, including $Pd_{3L}@Pd_1Ag_1$, Pd_1Ag_1, and Pd_{1L}-Ag_{sub} catalysts with different structures, are screened out to present better activity and selectivity toward gaseous C_2H_4 formation, especially Pd_1Ag_1 (the highest selectivity) and Pd_{1L}-Ag_{sub} (the highest activity).

Similarly, the projected density of states and the average Bader charge of the outermost Pd atoms over the $Pd_{3L}@Pd_1Ag_1$, Pd_1Ag_1, and Pd_{1L}-Ag_{sub} catalysts with better catalytic performance are also analyzed, in which the $Pd_{3L}@Pd_1Ag_1$ catalyst has lower catalytic performance compared to Pd_1Ag_1 and Pd_{1L}-Ag_{sub}. Further, although the activity of Pd_1Ag_1 is close to that of Pd_{1L}-Ag_{sub}, C_2H_4 selectivity on Pd_1Ag_1 is more than twice that on Pd_{1L}-Ag_{sub}; thus, taking C_2H_4 formation activity and selectivity into consideration, Pd_1Ag_1 has the best catalytic performance. As presented in Figure 9b, Pd_{1L}-Ag_{sub} with a moderate *d*-band center (−1.81 eV) shows superior activity than $Pd_{3L}@Pd_1Ag_1$ (−1.75 eV) and Pd_1Ag_1 (−2.53 eV). The average Bader charges for the outermost Pd atoms are −0.137 *e*, −0.071 *e*, and − 0.029 *e* on Pd_1Ag_1, Pd_{1L}-Ag_{sub}, and $Pd_{3L}@Pd_1Ag_1$, respectively; namely, Pd_1Ag_1 with the more Bader charges of outermost Pd atoms presents the best activity and selectivity of gaseous C_2H_4 formation.

Based on above analysis, among above 11 types of Pd-based alloy catalysts, taking C_2H_4 formation activity and selectivity into consideration, $Pd_{1L}@Pd_1Cu_3$, $Pd_{1L}@Ag$, $Pd_{2L}@Ag$, $Pd_{3L}@$

https://doi.org/10.1021/acs.jpcc.1c03157
J. Phys. Chem. C 2021, 125, 15251−15261

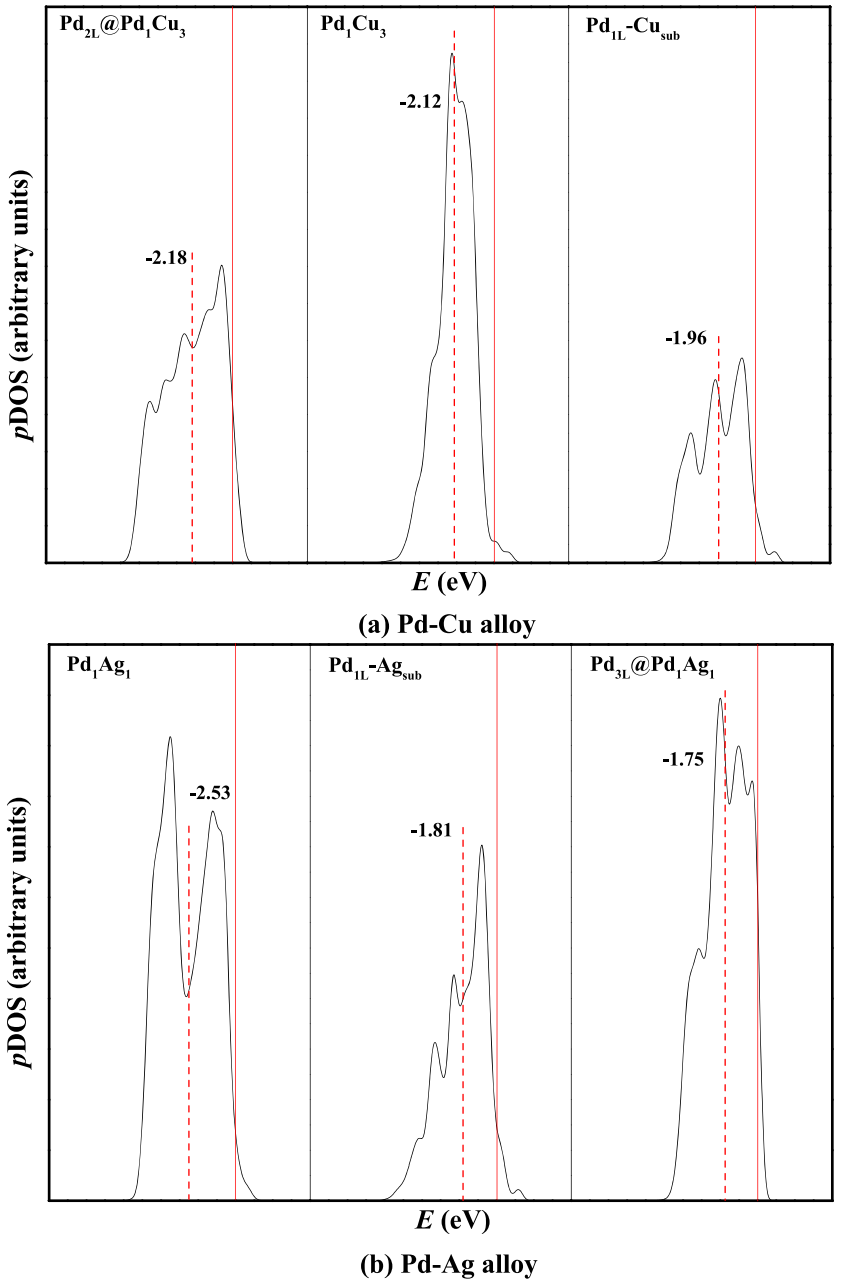

Figure 9. Projected density of states (PDOS) plots for the *d*-orbitals of the outmost layer atoms on the (a) Pd−Cu and (b) Pd−Ag alloy catalysts. The dashed red lines represent the location of the *d*-band center, and the solid red lines indicate the Fermi energy level to be zero.

Ag, and $Pd_{1L}@Pd_1Ag_1$ have poor catalytic performance for gaseous C_2H_4 formation, while $Pd_{2L}@Pd_1Cu_3$, Pd_1Cu_3, Pd_{1L}-Cu_{sub}, $Pd_{3L}@Pd_1Ag_1$, Pd_1Ag_1, and Pd_{1L}-Ag_{sub} show better catalytic performance, especially Pd_1Cu_3, Pd_1Ag_1, Pd_{1L}-Cu_{sub}, and Pd_{1L}-Ag_{sub}. Moreover, among the Pd−Cu and Pd−Ag alloy catalysts with better catalytic performances, a moderate distance between the Femi level and the *d*-band center leads to superior activity; the more the quantity of average Bader charges for the outermost Pd atoms is, the better the catalytic performance of gaseous C_2H_4 formation is.

Further, the microkinetic modeling has been widely used in C_2H_2 selective hydrogenation, and the effects of species coverage, temperature, and pressure on the catalytic performance are considered.[59−61] In this study, the microkinetic modeling is further implemented to probe into C_2H_4 formation activity and its selectivity in C_2H_2 selective hydrogenation on Pd-based catalysts under the typical experimental conditions (P_{C2H2} = 0.01 atm, P_{H2} = 0.1 atm, and T = 425 K). As presented in Figure 8, the Pd_1Cu_3, Pd_{1L}-Cu_{sub}, Pd_1Ag_1, and Pd_{1L}-Ag_{sub} catalysts are screened out to exhibit better activity and selectivity toward gaseous C_2H_4 formation; thus, the microkinetic modeling is conducted on these four catalysts (see details in the Supporting Information). As listed in Table S3, the C_2H_4 formation rates (s^{-1}·$site^{-1}$) on above four catalysts are in the sequence of Pd_1Cu_3 (4.64×10^{-11}) > Pd_{1L}-Cu_{sub} (6.57×10^{-14}) > Pd_{1L}-Ag_{sub} (3.49×10^{-14}) > Pd_1Ag_1 (1.64×10^{-16}), which agrees with the results obtained by the two-step model method. For the selectivity of C_2H_4, since the value of r_{C2H5} is much smaller than that of r_{C2H4}, the selectivity of C_2H_4 on these four catalysts are 100%, which is also consistent with the calculated results obtained by the difference between C_2H_4 hydrogenation and its desorption.

https://doi.org/10.1021/acs.jpcc.1c03157
J. Phys. Chem. C 2021, 125, 15251−15261

3.6.2. Influences of Surface Structures on Green Oil Production. Since green oil can block active centers and deactivate the catalyst in C_2H_2 selective hydrogenation, green oil production is further investigated on the Pd_1Cu_3, Pd_{1L}-Cu_{sub}, Pd_1Ag_1, and Pd_{1L}-Ag_{sub} catalysts with excellent activity and selectivity of gaseous C_2H_4 formation.

Our previously reported studies[40] found that the production of green oil on the Pd_1Cu_3 and Pd_1Ag_1 uniform alloy catalysts can be validly suppressed. For the Pd_{1L}-Cu_{sub} catalyst, see Figure S12a, compared to the routes of $C_2H_2 + C_2H_2$ (97.6 kJ·mol^{-1}) and $C_2H_2 + C_2H_3$ (46.9 kJ·mol^{-1}), the route of $C_2H_3 + C_2H_3$ (28.3 kJ·mol^{-1}) to produce 1,3-butadiene is the most advantageous in kinetics, which is also much easier in kinetics than the C_2H_4 desorption route (28.3 *vs* 81.6 kJ·mol^{-1}). For the Pd_{1L}-Ag_{sub} catalyst, see Figure S12b, the route of $C_2H_3 + C_2H_3$ to produce 1,3-butadiene is the most advantageous in kinetics (50.1 *vs* 101.9 and 74.7 kJ·mol^{-1}), which is also much easier in kinetics than the C_2H_4 desorption route (50.1 *vs* 93.4 kJ·mol^{-1}). Hence, green oil is easily formed on the subsurface structure of Pd_{1L}-Cu_{sub} and Pd_{1L}-Ag_{sub} catalysts.

Based on above results, it is concluded that both Pd_1Cu_3 and Pd_1Ag_1 catalysts with the uniform alloy surface structures not only display the superior activity and selectivity toward gaseous C_2H_4 formation but also effectively inhibit green oil formation. Thus, among the Pd-based alloy catalysts with four kinds of surface structures, the core−shell Pd_{nL}@M (M = Cu and Ag), core−shell Pd_{nL}@Pd_xM_y, the uniform alloys Pd_1Cu_3 and Pd_1Ag_1, and the subsurface structure Pd_{1L}-M_{sub}, it is concluded that engineering Pd-based alloy catalysts with the uniform alloy surface structure is the best choice for gaseous C_2H_4 formation in C_2H_2 selective hydrogenation.

3.6.3. Influences of Subsurface Hydrogen on C_2H_4 Formation Activity and Selectivity. For the Pd catalyst, since previous studies by Yang *et al.*[57] have shown that the presence of subsurface hydrogen significantly changes the reactivity and selectivity toward C_2H_2 selective hydrogenation on Pd surfaces, the effect of subsurface hydrogen on the C_2H_4 formation activity and selectivity is investigated over the uniform alloy Pd_1Cu_3 and Pd_1Ag_1 catalysts with excellent catalytic performance toward C_2H_4 formation.

For the Pd_1Cu_3 catalyst, as shown in Figure S13, four types of subsurface adsorption sites are considered; when H is initially adsorbed at the tetrahedron 1 (TET1) site and octahedron 2 (OCT2) site, the optimized structure showed that the H atom diffuses from the subsurface to the surface; when H is adsorbed at the TET2 and OCT1 sites, H is still located at the subsurface sites after optimization; however, as listed in Table S4, the adsorption ability of the H atom at the OCT1 site is stronger than that at the TET2 site, so the stable adsorption site of H at the subsurface is the OCT1 site. Similarly, on the Pd_1Ag_1 catalyst, the stable adsorption site of H at the subsurface is the OCT1 site. Thus, according to the previous studies by Yang *et al.*,[57] both Pd_1Cu_3(111) and Pd_1Ag_1(111) surfaces with 1 monolayer (ML) of H atoms at the stable subsurface adsorption sites (named as Pd_1Cu_3/H_{sub} and Pd_1Ag_1/H_{sub}) are employed to clarify the effect of subsurface H on C_2H_4 formation activity and selectivity (see details in the Supporting Information).

As shown in Figure S14, the C_2H_4 desorption route is preferred on Pd_1Cu_3/H_{sub} and Pd_1Ag_1/H_{sub}; meanwhile, as listed in Table 1, C_2H_4 selectivity is 54.7 kJ·mol^{-1} on Pd_1Cu_3/H_{sub}, which is close to that on Pd_1Cu_3 (51.9 kJ·mol^{-1}); however, the activity of C_2H_4 formation on Pd_1Cu_3/H_{sub} is much lower than that of Pd_1Cu_3 (8.21×10^0 *vs* 8.65×10^6 s^{-1}·site^{-1}); thus, the presence of subsurface H on the Pd_1Cu_3 catalyst decreases the activity of gaseous C_2H_4 formation. For Pd_1Ag_1/H_{sub}, C_2H_4 selectivity is 65.6 kJ·mol^{-1}, which is slightly higher than that on Pd_1Ag_1 (59.6 kJ·mol^{-1}); meanwhile, the activity is 4.37×10^1 s^{-1}·site^{-1}, which is higher than that on Pd_1Ag_1 (1.09×10^1 s^{-1}·site^{-1}); thus, the presence of subsurface H on the Pd_1Ag_1 catalyst promotes C_2H_4 formation activity and selectivity.

Table 1. Adsorption Free Energies (G_{ads}/kJ·mol^{-1}) of C_2H_4, the Activation Barriers (G_a/kJ·mol^{-1}) of C_2H_4 Hydrogenation to C_2H_5, C_2H_4 Selectivity (G_{sel}/kJ·mol^{-1}), and the Rate of C_2H_4 Formation (r/s^{-1}·site^{-1}) in C_2H_2 Selective Hydrogenation over the Pd-Based Alloy Catalysts at 425 K

catalysts	$G_{ads}(C_2H_4)$	G_a	G_{sel}	r
Pd_{1L}@Cu	−49.8	93.9	—	—
Pd_{1L}@Pd_1Cu_3	−40.9	95.6	54.7	1.08×10^{-1}
Pd_{2L}@Pd_1Cu_3	−73.5	92.7	19.2	1.46×10^{0}
Pd_{3L}@Pd_1Cu_3	−69.8	87.1	—	—
Pd_{1L}@Ag	−55.7	111.8	56.1	4.89×10^{-2}
Pd_{2L}@Ag	−77.4	106.7	29.3	4.96×10^{-6}
Pd_{3L}@Ag	−71.9	106.9	35.0	2.89×10^{-3}
Pd_{1L}@Pd_1Ag_1	−71.5	114.4	42.9	5.65×10^{-5}
Pd_{2L}@Pd_1Ag_1	−71.8	99.6	—	—
Pd_{3L}@Pd_1Ag_1	−71.3	103.4	32.1	1.56×10^{-1}
Pd_1Cu_3	−45.5	97.4	51.9	8.65×10^{6}
Pd_1Ag_1	−49.3	108.9	59.6	1.09×10^{1}
Pd_{1L}-Cu_{sub}	−40.2	95.1	54.9	8.28×10^{2}
Pd_{1L}-Ag_{sub}	−58.4	88.0	29.6	2.93×10^{1}
Pd_1Cu_3/H_{sub}	−84.0	138.7	54.7	8.21×10^{0}
Pd_1Ag_1/H_{sub}	−50.3	115.9	65.6	4.37×10^{1}

4. CONCLUSIONS

In this work, the catalytic performance of gaseous C_2H_4 formation in C_2H_2 selective hydrogenation on Pd-based alloy catalysts are fully investigated using DFT calculations; here, four kinds of surface structures, including the core−shell Pd_{nL}@M (M = Cu and Ag), the core−shell Pd_{nL}@Pd_xM_y, the uniform alloys Pd_1Cu_3 and Pd_1Ag_1, and the subsurface structure Pd_{1L}-M_{sub}, are engineered to reveal the influences of the surface structures on the gaseous C_2H_4 formation activity and selectivity. The results show that the surface structures of Pd-based alloy catalysts significantly affect the activity and selectivity of gaseous C_2H_4 formation on all considered Pd-based alloy catalysts. Among them, the Pd_1Cu_3, Pd_{1L}-Cu_{sub}, Pd_1Ag_1, and Pd_{1L}-Ag_{sub} catalysts are screened out to serve as four promising candidates in the hydrogenation process, which exhibit better activity and selectivity toward gaseous C_2H_4 formation, especially Pd_1Cu_3 and Pd_1Ag_1 with the uniform alloy structure. However, in the polymerization process, green oil is easily formed on the Pd_{1L}-Cu_{sub} and Pd_{1L}-Ag_{sub} catalysts. Namely, only the uniform alloy surface structures, Pd_1Cu_3 and Pd_1Ag_1, are the most suitable choice among all considered Pd-based alloy catalysts for C_2H_2 selective hydrogenation to C_2H_4, which not only can exhibit excellent activity and selectivity toward gaseous C_2H_4 formation but also effectively suppress green oil production; moreover, both the intermetallic Pd_1Cu_3 and Pd_1Ag_1 alloy catalysts have great thermal stability. This study could serve as an example of rationally engineering the surface structure of

https://doi.org/10.1021/acs.jpcc.1c03157
J. Phys. Chem. C 2021, 125, 15251−15261

Pd-based alloy catalysts in C_2H_2 selective hydrogenation, which may be applied to the design of other types of catalysts.

■ ASSOCIATED CONTENT

Supporting Information

The Supporting Information is available free of charge at https://pubs.acs.org/doi/10.1021/acs.jpcc.1c03157.

The detailed descriptions about the calculations of C_2H_4 formation activity and selectivity (Part 1), the adsorption of H and C_2H_x (x = 2−5) species (Parts 2 and 3), H_2 dissociation (Part 4), free-energy profiles of C_2H_2 selective hydrogenation (Part 5), microkinetic modeling (Part 6), green oil formation analysis (Part 7), H adsorption at the subsurface sites of Pd_1Cu_3 and Pd_1Ag_1 (Part 8), and the free-energy profiles on Pd_1Cu_3/H_{sub} and Pd_1Ag_1/H_{sub} (Part 9) are presented (PDF)

■ AUTHOR INFORMATION

Corresponding Author

Riguang Zhang − *State Key Laboratory of Clean and Efficient Coal Utilization, Taiyuan University of Technology, Taiyuan 030024 Shanxi, P.R. China; Key Laboratory of Coal Science and Technology, Ministry of Education, Taiyuan University of Technology, Taiyuan 030024, China;* orcid.org/0000-0001-8956-8425; Email: zhangriguang@tyut.edu.cn, zhangriguang1981@163.com

Authors

Wenjuan Zheng − *State Key Laboratory of Clean and Efficient Coal Utilization, Taiyuan University of Technology, Taiyuan 030024 Shanxi, P.R. China; Key Laboratory of Coal Science and Technology, Ministry of Education, Taiyuan University of Technology, Taiyuan 030024, China*

Yuan Wang − *State Key Laboratory of Clean and Efficient Coal Utilization, Taiyuan University of Technology, Taiyuan 030024 Shanxi, P.R. China; Key Laboratory of Coal Science and Technology, Ministry of Education, Taiyuan University of Technology, Taiyuan 030024, China*

Baojun Wang − *State Key Laboratory of Clean and Efficient Coal Utilization, Taiyuan University of Technology, Taiyuan 030024 Shanxi, P.R. China; Key Laboratory of Coal Science and Technology, Ministry of Education, Taiyuan University of Technology, Taiyuan 030024, China;* orcid.org/0000-0002-9069-6720

Maohong Fan − *Departments of Chemical and Petroleum Engineering, University of Wyoming, Laramie, Wyoming 82071, United States; School of Civil and Environmental Engineering, Georgia Institute of Technology, Atlanta, Georgia 30332, United States; School of Energy Resources, University of Wyoming, Laramie, Wyoming 82071, United States;* orcid.org/0000-0003-1334-7292

Lixia Ling − *State Key Laboratory of Clean and Efficient Coal Utilization, Taiyuan University of Technology, Taiyuan 030024 Shanxi, P.R. China; Key Laboratory of Coal Science and Technology, Ministry of Education, Taiyuan University of Technology, Taiyuan 030024, China*

Complete contact information is available at: https://pubs.acs.org/10.1021/acs.jpcc.1c03157

Author Contributions

#W.Z. and Y.W. contributed equally to this work.

Notes

The authors declare no competing financial interest.

■ ACKNOWLEDGMENTS

This work is financially supported by the National Natural Science Foundation of China (nos. 21776193 and 22078221).

■ REFERENCES

(1) Zhao, Z. J.; Zhao, J.; Chang, X.; Zha, S.; Zeng, L.; Gong, J. Competition of C-C Bond Formation and C-H Bond Formation for Acetylene Hydrogenation on Transition Metals: A Density Functional Theory Study. *AIChE J.* **2019**, *65*, 1059−1066.

(2) Vignola, E.; Steinmann, S. N.; Al Farra, A.; Vandegehuchte, B. D.; Curulla, D.; Sautet, P. Evaluating the Risk of C-C Bond Formation during Selective Hydrogenation of Acetylene on Palladium. *ACS Catal.* **2018**, *8*, 1662−1671.

(3) Yang, C.; Wang, G.; Liang, A.; Yue, Y.; Peng, H.; Cheng, D. Understanding the Role of Au in the Selective Hydrogenation of Acetylene on Trimetallic PdAgAu Catalytic Surface. *Catal. Commun.* **2019**, *124*, 41−45.

(4) McCue, A. J.; Anderson, J. A. Recent Advances in Selective Acetylene Hydrogenation Using Palladium Containing Catalysts. *Front. Chem. Sci. Eng.* **2015**, *9*, 142−153.

(5) Leviness, S.; Nair, V.; Weiss, A. H.; Schay, Z.; Guczi, L. Acetylene Hydrogenation Selectivity Control on $PdCu/Al_2O_3$ Catalysts. *J. Mol. Catal.* **1984**, *25*, 131−140.

(6) Zhang, R.; Zhao, B.; Ling, L.; Wang, A.; Russell, C. K.; Wang, B.; Fan, M. Cost-Effective Palladium-Doped Cu Bimetallic Materials to Tune Selectivity and Activity by Using Doped Atom Ensembles as Active Sites for Efficient Removal of Acetylene from Ethylene. *ChemCatChem* **2018**, *10*, 2424−2432.

(7) Pei, G. X.; Liu, X. Y.; Yang, X.; Zhang, L.; Wang, A.; Li, L.; Wang, H.; Wang, X.; Zhang, T. Performance of Cu-Alloyed Pd Single-Atom Catalyst for Semihydrogenation of Acetylene under Simulated Front-End Conditions. *ACS Catal.* **2017**, *7*, 1491−1500.

(8) Kim, S. K.; Lee, J. H.; Ahn, I. Y.; Kim, W. J.; Moon, S. H. Performance of Cu-Promoted Pd Catalysts Prepared by Adding Cu Using a Surface Redox Method in Acetylene Hydrogenation. *Appl. Catal. A-Gen.* **2011**, *401*, 12−19.

(9) Meng, L. D.; Wang, G. C. A DFT+U Study of Acetylene Selective Hydrogenation over Anatase Supported Pd_aAg_b(a+b=4) Cluster. *Phys. Chem. Chem. Phys.* **2014**, *16*, 17541−17550.

(10) Mei, D.; Neurock, M.; Smith, C. M. Hydrogenation of Acetylene-Ethylene Mixtures over Pd and Pd-Ag Alloys: First-Principles-Based Kinetic Monte Carlo Simulations. *J. Catal.* **2009**, *268*, 181−195.

(11) Sárkány, A.; Horváth, A.; Beck, A. Hydrogenation of Acetylene over Low Loaded Pd and $Pd-Au/SiO_2$ Catalysts. *Appl. Catal. A-Gen.* **2002**, *229*, 117−125.

(12) Zhang, Y.; Diao, W.; Williams, C. T.; Monnier, J. R. Selective Hydrogenation of Acetylene in Excess Ethylene Using Ag- and Au-Pd/SiO_2 Bimetallic Catalysts Prepared by Electroless Deposition. *Appl. Catal. A-Gen.* **2014**, *469*, 419−426.

(13) Ma, C.; Du, Y.; Feng, J.; Cao, X.; Yang, J.; Li, D. Fabrication of Supported PdAu Nanoflower Catalyst for Partial Hydrogenation of Acetylene. *J. Catal.* **2014**, *317*, 263−271.

(14) Zhou, H.; Yang, X.; Li, L.; Liu, X.; Huang, Y.; Pan, X.; Wang, A.; Li, J.; Zhang, T. PdZn Intermetallic Nanostructure with Pd-Zn-Pd Ensembles for Highly Active and Chemoselective Semi-Hydrogenation of Acetylene. *ACS Catal.* **2016**, *6*, 1054−1061.

(15) Feng, Q. C.; Zhao, S.; Wang, Y.; Dong, J. C.; Chen, W. X.; He, D. S.; Wang, D. S.; Yang, J.; Zhu, Y. M.; Zhu, H. L.; et al. Isolated Single-Atom Pd Sites in Intermetallic Nanostructures: High Catalytic Selectivity for Semihydrogenation of Alkynes. *J. Am. Chem. Soc.* **2017**, *139*, 7294−7301.

(16) Núria, L.; Crisa, V. F. Promoters in the Hydrogenation of Alkynes in Mixtures: Insights from Density Functional Theory. *Chem. Commun.* **2012**, *48*, 1379−1391.

(17) Vignola, E.; Steinmann, S. N.; Le Mapihan, K.; Vandegehuchte, B. D.; Curulla, D.; Sautet, P. Acetylene Adsorption on Pd−Ag Alloys: Evidence for Limited Island Formation and Strong Reverse Segregation from Monte Carlo Simulations. *J. Phys. Chem. C* **2018**, *122*, 15456−15463.
(18) Ravanchi, M. T.; Sahebdelfar, S.; Komeili, S. Acetylene Selective Hydrogenation: A Technical Review on Catalytic Aspects. *Rev. Chem. Eng.* **2018**, *34*, 215−237.
(19) Tsai, H. C.; Hsieh, Y. C.; Yu, T. H.; Lee, Y. J.; Wu, Y. H.; Merinov, B. V.; Wu, P. W.; Chen, S. Y.; Adzic, R. R.; Goddard, W. A., III DFT Study of Oxygen Reduction Reaction on Os/Pt Core-Shell Catalysts Validated by Electrochemical Experiment. *ACS Catal.* **2015**, *5*, 1568−1580.
(20) Kim, Y.; Hong, J. W.; Lee, Y. W.; Kim, M.; Kim, D.; Yun, W. S.; Han, S. W. Synthesis of AuPt Heteronanostructures with Enhanced Electrocatalytic Activity toward Oxygen Reduction. *Angew. Chem., Int. Ed.* **2010**, *49*, 10197−10201.
(21) Dai, C.; Yang, Y.; Zhao, Z.; Fisher, A.; Liu, Z.; Cheng, D. From Mixed to Three-Layer Core/Shell PtCu Nanoparticles: Ligand-Induced Surface Segregation to Enhance Electrocatalytic Activity. *Nanoscale* **2017**, *9*, 8945−8951.
(22) Ferreira de Morais, R.; Franco, A. A.; Sautet, P.; Loffreda, D. How Does the Surface Structure of Pt-Ni Alloys Control Water and Hydrogen Peroxide Formation? *ACS Catal.* **2016**, *6*, 5641−5650.
(23) Bueno, S. L. A.; Ashberry, H. M.; Shafei, I.; Skrabalak, S. E. Building Durable Multimetallic Electrocatalysts from Intermetallic Seeds. *Acc. Chem. Res.* **2021**, *54*, 1662−1672.
(24) Yang, H.; Wang, K.; Tang, Z.; Liu, Z.; Chen, S. Bimetallic PdZn Nanoparticles for Oxygen Reduction Reaction in Alkaline Medium: The Effects of Surface Structure. *J. Catal.* **2020**, *382*, 181−191.
(25) Kang, Y.; Qi, L.; Li, M.; Diaz, R. E.; Su, D.; Adzic, R. R.; Stach, E.; Li, J.; Murray, C. B. Highly Active Pt_3Pb and Core-Shell Pt_3Pb-Pt Electrocatalysts for Formic Acid Oxidation. *ACS Nano* **2012**, *6*, 2818−2825.
(26) Xie, S. F.; Choi, S.-I.; Lu, N.; Roling, L. T.; Herron, J. A.; Zhang, L.; Park, J.; Wang, J. G.; Kim, M. J.; Xie, Z. X.; et al. Atomic Layer-by-Layer Deposition of Pt on Pd Nanocubes for Catalysts with Enhanced Activity and Durability toward Oxygen Reduction. *Nano Lett.* **2014**, *14*, 3570−3576.
(27) Yang, Y.; Xu, H.; Cao, D.; Zeng, X. C.; Cheng, D. Hydrogen Production via Efficient Formic Acid Decomposition: Engineering the Surface Structure of Pd-Based Alloy Catalysts by Design. *ACS Catal.* **2019**, *9*, 781−790.
(28) Takht Ravanchi, M.; Fadaeerayeni, S.; Rahimi Fard, M. An Egg-Shell Pd-Ag/α-Al_2O_3 Catalyst for Tail-End Acetylene Selective Hydrogenation. *Iran. J. Chem. Eng.* **2014**, *11*, 42−54.
(29) Sárkány, A.; Geszti, O.; Sáfrán, G. Preparation of Pd_{shell}−Au_{core}/SiO_2 Catalyst and Catalytic Activity for Acetylene Hydrogenation. *Appl. Catal. A-Gen.* **2008**, *350*, 157−163.
(30) Zuo, Z. J.; Gao, X. Y.; Han, P. D.; Liu, S. Z.; Huang, W. Density Functional Theory (DFT) and Kinetic Monte Carlo (KMC) Study of the Reaction Mechanism of Hydrogen Production from Methanol on ZnCu(111). *J. Phys. Chem. C* **2016**, *120*, 27500−27508.
(31) Zhang, R.; Zhang, J.; Jiang, Z.; Wang, B.; Fan, M. The Cost-Effective Cu-Based Catalysts for the Efficient Removal of Acetylene from Ethylene: The Effects of Cu Valence State, Surface Structure and Surface Alloying on the Selectivity and Activity. *Chem. Eng. J.* **2018**, *351*, 732−746.
(32) Hammer, B.; Hansen, L. B.; Nørskov, J. K. Improved Adsorption Energetics within Density-Functional Theory Using Revised Perdew-Burke-Ernzerhof Functionals. *Phys. Rev. B* **1999**, *59*, 7413−7421.
(33) Perdew, J. P.; Burke, K.; Ernzerhof, M. Generalized Gradient Approximation Made Simple. *Phys. Rev. Lett.* **1996**, *77*, 3865−3868.
(34) Inada, Y.; Orita, H. Efficiency of Numerical Basis Sets for Predicting the Binding Energies of Hydrogen Bonded Complexes: Evidence of Small Basis Set Superposition Error Compared to Gaussian Basis Sets. *J. Comput. Chem.* **2008**, *29*, 225−232.
(35) Zhou, C.; Wu, J.; Nie, A.; Forrey, R. C.; Tachibana, A.; Cheng, H. On the Sequential Hydrogen Dissociative Chemisorption on Small Platinum Clusters: A Density Functional Theory Study. *J. Phys. Chem. C* **2007**, *111*, 12773−12778.
(36) Wang, B.; Song, L.; Zhang, R. The Dehydrogenation of CH_4 On Rh(111), Rh(110) and Rh(100) Surfaces: A Density Functional Theory Study. *Appl. Surf. Sci.* **2012**, *258*, 3714−3722.
(37) Chen, X. M.; Yang, B.; Tao, D. P.; Dai, Y. N. Theory Study of AlCl Disproportionation Reaction Mechanism on Al(110) Surface. *Metall. Mater. Trans. B* **2010**, *41*, 137−145.
(38) Armbrüster, M.; Kovnir, K.; Behrens, M.; Teschner, D.; Grin, Y.; Schlögl, R. Pd-Ga Intermetallic Compounds as Highly Selective Semihydrogenation Catalysts. *J. Am. Chem. Soc.* **2010**, *132*, 14745−14747.
(39) Borodziński, A.; Bond, G. C. Selective Hydrogenation of Ethyne in Ethene-Rich Streams on Palladium Catalysts. Part 1. Effect of Changes to the Catalyst during Reaction. *Catal. Rev. Sci. Eng.* **2006**, *48*, 91−144.
(40) Wang, Y.; Zheng, W.; Wang, B.; Ling, L.; Zhang, R. The Effects of Doping Metal Type and Ratio on the Catalytic Performance of C_2H_2 Semi-Hydrogenation over the Intermetallic Compound-Containing Pd Catalysts. *Chem. Eng. Sci.* **2021**, *229*, 116131.
(41) Wang, Y.; Wang, B.; Ling, L.; Zhang, R.; Fan, M. Probe into the Effects of Surface Composition and Ensemble Effect of Active Sites on the Catalytic Performance of C_2H_2 Semi-Hydrogenation over the Pd-Ag Bimetallic Catalysts. *Chem. Eng. Sci.* **2020**, *218*, 115549.
(42) Xu, L.; Stangland, E. E.; Mavrikakis, M. Ethylene versus Ethane: A DFT-Based Selectivity Descriptor for Efficient Catalyst Screening. *J. Catal.* **2018**, *362*, 18−24.
(43) Xu, Z. N.; Sun, J.; Lin, C. S.; Jiang, X. M.; Chen, Q. S.; Peng, S. Y.; Wang, M. S.; Guo, G. C. High-Performance and Long-Lived Pd Nanocatalyst Directed by Shape Effect for CO Oxidative Coupling to Dimethyl Oxalate. *ACS Catal.* **2013**, *3*, 118−122.
(44) Kim, S. K.; Kim, C.; Lee, J. H.; Kim, J.; Lee, H.; Moon, S. H. Performance of Shape-Controlled Pd Nanoparticles in the Selective Hydrogenation of Acetylene. *J. Catal.* **2013**, *306*, 146−154.
(45) Filoti, D. I.; Bedell, A. R.; Harper, J. M. E. Synergistic Ag(111) and Cu(111) Texture Evolution in Phase-Segregated $Cu_{1-x}Ag_x$ Magnetron Sputtered Composite Thin Films. *J. Vac. Sci. Technol., A* **2010**, *28*, 838−841.
(46) Zheng, H.; Zhang, R.; Li, Z.; Wang, B. Insight into the Mechanism and Possibility of Ethanol Formation from Syngas on Cu(100) Surface. *J. Mol. Catal. A: Chem.* **2015**, *404-405*, 115−130.
(47) Peljhan, S.; Kokalj, A. DFT Study of Gas-Phase Adsorption of Benzotriazole on Cu(111), Cu(100), Cu(110), and Low Coordinated Defects Thereon. *Phys. Chem. Chem. Phys.* **2011**, *13*, 20408−20417.
(48) Bridier, B.; López, N.; Pérez-Ramírez, J. Molecular Understanding of Alkyne Hydrogenation for the Design of Selective Catalysts. *Dalton Trans.* **2010**, *39*, 8412−8419.
(49) Yang, B.; Burch, R.; Hardacre, C.; Hu, P.; Hughes, P. Mechanistic Study of 1,3-Butadiene Formation in Acetylene Hydrogenation over the Pd-Based Catalysts Using Density Functional Calculations. *J. Phys. Chem. C* **2014**, *118*, 1560−1567.
(50) Studt, F.; Abild-Pedersen, F.; Bligaard, T.; Sørensen, R. Z.; Christensen, C. H.; Nørskov, J. K. On the Role of Surface Modifications of Palladium Catalysts in the Selective Hydrogenation of Acetylene. *Am. Ethnol.* **2008**, *120*, 9439−9442.
(51) Yang, B.; Burch, R.; Hardacre, C.; Hu, P.; Hughes, P. Selective Hydrogenation of Acetylene over Cu(211), Ag(211) and Au(211): Horiuti-Polanyi Mechanism: Vs. Non-Horiuti-Polanyi Mechanism. *Catal. Sci. Technol.* **2017**, *7*, 1508−1514.
(52) Studt, F.; Abild-Pedersen, F.; Bligaard, T.; Sørensen, R. Z.; Christensen, C. H.; Nørskov, J. K. Identification of Non-Precious Metal Alloy Catalysts for Selective Hydrogenation of Acetylene. *Science* **2008**, *320*, 1320−1322.
(53) Ma, H. Y.; Wang, G. C. Selective Hydrogenation of Acetylene on Pt_n/TiO_2 (N=1, 2, 4, 8) Surfaces: Structure Sensitivity Analysis. *ACS Catal.* **2020**, *10*, 4922−4928.

https://doi.org/10.1021/acs.jpcc.1c03157
J. Phys. Chem. C 2021, 125, 15251−15261

(54) Yang, B.; Burch, R.; Hardacre, C.; Headdock, G.; Hu, P. Origin of the Increase of Activity and Selectivity of Nickel Doped by Au, Ag, and Cu for Acetylene Hydrogenation. *ACS Catal.* **2012**, *2*, 1027−1032.
(55) Zhang, R.; Zhang, J.; Zhao, B.; He, L.; Wang, A.; Wang, B. Insight into the Effects of Cu Component and the Promoter on the Selectivity and Activity for Efficient Removal of Acetylene from Ethylene on Cu-Based Catalyst. *J. Phys. Chem. C* **2017**, *121*, 27936−27949.
(56) Zhang, R.; Zhao, B.; He, L.; Wang, A.; Wang, B. Cost-Effective Promoter-Doped Cu-Based Bimetallic Catalysts for the Selective Hydrogenation of C_2H_2 to C_2H_4: The Effect of the Promoter on Selectivity and Activity. *Phys. Chem. Chem. Phys.* **2018**, *20*, 17487−17496.
(57) Yang, B.; Burch, R.; Hardacre, C.; Headdock, G.; Hu, P. Influence of Surface Structures, Subsurface Carbon and Hydrogen, and Surface Alloying on the Activity and Selectivity of Acetylene Hydrogenation on Pd Surfaces: A Density Functional Theory Study. *J. Catal.* **2013**, *305*, 264−276.
(58) Zhao, B.; Zhang, R.; Huang, Z.; Wang, B. Effect of the Size of Cu Clusters on Selectivity and Activity of Acetylene Selective Hydrogenation. *Appl. Catal. A-Gen.* **2017**, *546*, 111−121.
(59) Gonçalves, L. P. L.; Wang, J. G.; Vinati, S.; Barborini, E.; Wei, X. K.; Heggen, M.; Franco, M.; Sousa, J. P. S.; Petrovykh, D. Y.; Soares, O. S. G. P.; et al. Combined Experimental and Theoretical Study of Acetylene Semi-Hydrogenation over Pd/Al_2O_3. *Int. J. Hydrogen Energy* **2020**, *45*, 1283−1296.
(60) Yang, J.; Lv, C. Q.; Guo, Y.; Wang, G. C. A DFT+U Study of Acetylene Selective Hydrogenation on Oxygen Defective Anatase (101) and Rutile (110) TiO_2 Supported Pd_4 Cluster. *J. Chem. Phys.* **2012**, *136*, 104107.
(61) Ayodele, O. B.; Cai, R. S.; Wang, J. G.; Ziouani, Y.; Liang, Z. F.; Spadaro, M. C.; Kovnir, K.; Arbiol, J.; Akola, J.; Palmer, R. E.; et al. Synergistic Computational-experimental Discovery of Highly Selective PtCu Nanocluster Catalysts for Acetylene Semihydrogenation. *ACS Catal.* **2020**, *10*, 451−457.

https://doi.org/10.1021/acs.jpcc.1c03157
J. Phys. Chem. C 2021, 125, 15251−15261